Feasibility Study of a Photodetector with 10 Picosecond Time Resolution for a Fast-Timing Subsystem in the ATLAS Detector at the LHC

Todd Seiss
Adviser: Henry Frisch

June 13, 2016

Abstract

One of the major problems facing detectors at the High Luminosity LHC is event separation when there are a large number of simultaneous events. Large Area Picosecond Photo-Detectors are very fast-timing, modular photodetectors with a photosensitive area of 20 cm by 20 cm per module that may be useful to solve this problem. I examined their possible use for the ATLAS High-Granularity Timing Detector, which would be placed in front of the forward electromagnetic calorimeter in the Phase II upgrade. Timing resolution would provide event separation in this region, since vertexing is difficult. To mitigate the high event rates and provide position resolution, it is necessary to segment the large area, which can be accomplished with a new photodetector design that allows a highly segmented readout. In this design, called the "inside-out" configuration, the anode inside the vacuum of the detector is a thin, grounded layer of a resistive conductor, such as nichrome. The pulses from the electron shower can then be read through the ceramic detector base via capacitive coupling to the anode layer, transmitting the signal to the outside of the vacuum without a DC connection. This allows custom readout designs to be easily implemented. I demonstrate the effectiveness of pads in the inside-out configuration, and I measure the position and time resolution, applying these results to ATLAS by comparing to Pythia simulations. This thereby shows that to have a sufficiently low event rate that the detector is not saturated, pad sizes need to be on the order of millimeters, corresponding to 10^4 or 10^5 readout channels.

Contents

1 Introduction

1.1 Fast Timing in a Collider Detector

1.1.1 Forward Pileup Mitigation with Fast-Timing

In the mid-2020's, the Large Hadron Collider (LHC) is scheduled for a major upgrade to the high-luminosity LHC. After the upgrade, the number of collisions per bunch crossing [App. A[1]] will increase to roughly 200. Thus a major problem is to disentangle these 200 messy events.

For particles in the central region [App. A] of the detector, this problem will be mitigated by accurate vertexing [App. A]. By tracking particles precisely, it is possible to identify and discriminate different vertices. Vertexing, however, only works well when the particle trajectories are approximately transverse, so that a small change in trajectory angle corresponds to a small change in reconstructed position.

In the forward region [App. A], where the particles are close to the direction of the beam, tracking is very difficult. A small change in track position results in a large change in reconstructed vertex position, so particle tracking is not a good discrimination method.

Instead, one can use relative timing between the arrival times of different particles. The interaction region is roughly 20 cm long, which corresponds to a time of flight of approximately 600 picoseconds. Thus measuring arrival times with picosecond resolution can mitigate forward pileup.

One problem with operating a detector in the forward region is the much higher particle flux compared to the central region. If the pixel of a detector is too large, it will be triggered by several events per bunch crossing and will not be able to distinguish different events. Thus this problem can be solved by making the pixels small so that only a fraction of them trigger per bunch crossing.

1.1.2 ATLAS and the High Granularity Timing Detector (HGTD)

ATLAS is one of the two general purpose particle detectors at the LHC. Within the ATLAS collaboration, there is a project studying the addition of a fast-timing, granular detector in the forward region, called the high granularity timing detector (HGTD) [3]. This detector is to be placed in front of the forward electromagnetic calorimeters to enable fast timing and position resolution in this region. Figure 1 is a drawing of ATLAS with the HGTD location marked.

The HGTD would be placed at $z \approx 3.5$ m [App. A], and it would span roughly the range of radii 9 cm $< R <$ 60 cm [3]. Equivalently, it spans the range $2.4 < \eta < 4.3$ where η is pseudorapidity [App. A].

[1] Throughout, [App. A] will indicate "see Appendix A for a definition."

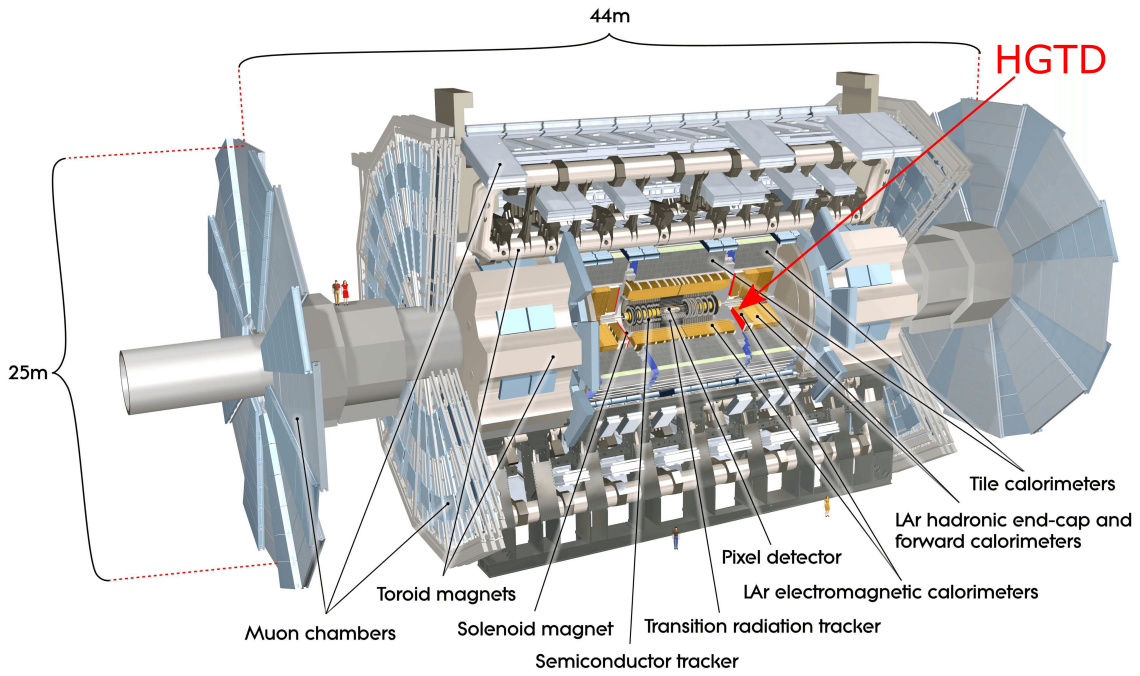

Figure 1: A slice of the ATLAS detector [2]. The High Granularity Timing Detector (HGTD) is shown in red.

1.2 Large-Area Picosecond Photodetectors (LAPPD's) and the Inside-Out Configuration

Large-Area Picosecond Photodetectors (LAPPD's) are a developing photodetector technology that allows for fast timing on the order of picoseconds over an area of 20 cm $\times$ 20 cm [4]. In an LAPPD, a photon enters through the top window impacting a photocathode and ejects a photoelectron. A high voltage on the photocathode causes the photocathode to be accelerated toward the microchannel plates (MCP's). MCP's are porous plates with pore diameters on the order of 10 microns [4]. The photoelectron enters a channel, impacting the wall and ejecting more electrons. These electrons are accelerated by the high voltage and impact a wall again, ejecting more electrons. This multiplication happens roughly 10 times over a distance of millimeters, over 2 MCP's, producing a large shower of electrons with a gain typically on the order of 10^6 [4]. The process is shown schematically in Figure 1.2.

Because this happens over a short distance, compared to the few inches of photomultiplication in a traditional photomultiplier tube, the time resolution is improved. LAPPD's will achieve time resolution on the order of picoseconds, compared to roughly 100 picoseconds for photomultiplier tubes.

LAPPD's are intended to have picosecond fast-timing, a large area, and a relatively inexpensive price compared to other MCP detectors, and they are expected to operate in

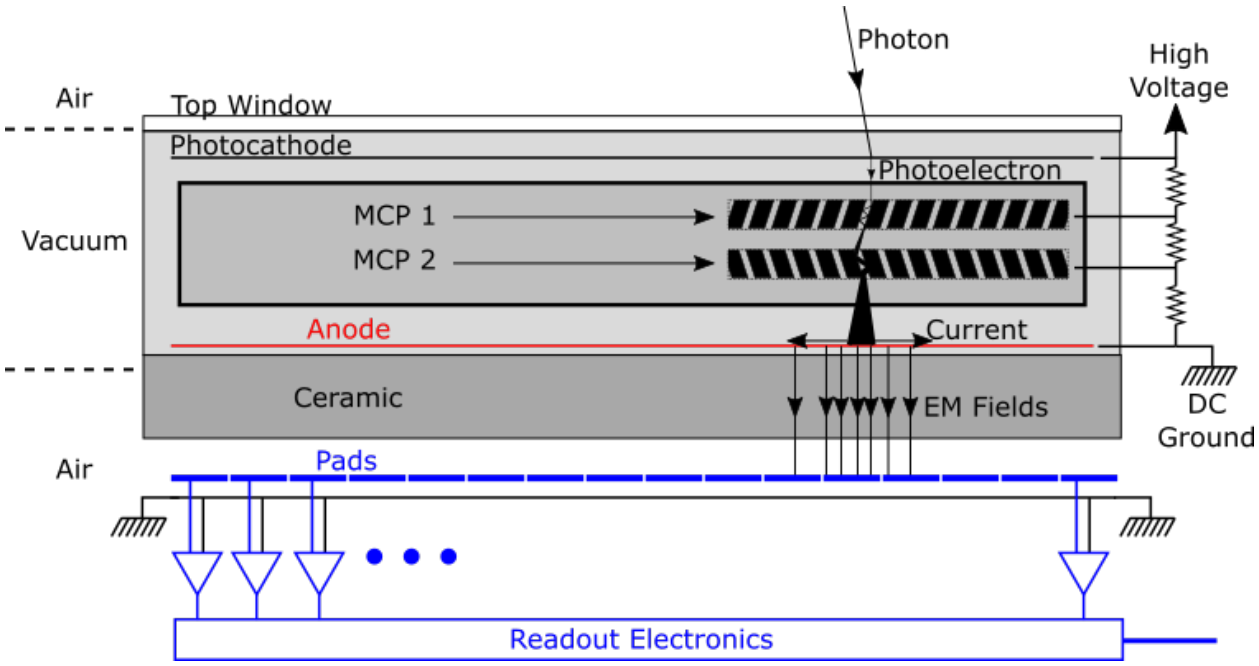

Figure 2: A sketch of an inside-out LAPPD. An incoming photon passes through the top window and ejects a photoelectron from the photocathode. The photoelectron enters the microchannel plates and is multiplied to an electron shower. This shower impacts an inner anode layer, producing a pulse of current. The current induces fields that are picked up with the pads readout outside the vacuum.

high magnetic fields. They thus seem well-suited for fast-timing in a collider detector.[2] One problem with LAPPD's for colliders is that in the current design, they are not sufficiently granular, a necessary feature discussed above. However, this problem is solved with the inside-out configuration.

1.3 Inside-Out Configuration

When an electron shower approaches the anode, positive charge is drawn toward the shower, resulting in a flow of electrons away from the shower. When the shower reaches the anode, it neutralizes with the positive charge in the center, while the current persists and continues to flow outward. In a conventional configuration, the anode would be some arrangement of good conductors, and these currents could be read out. This has many disadvantages. First, the anode is inside the vacuum of the detector, so each channel requires a separate readout through the vacuum wall. Additionally, changing the anode configuration require building another LAPPD with a different anode, possibly with a different process. The readout is

[2]To detect a charged particle with an LAPPD, one can place, for example, a quartz window immediately in front of the photosensitive area. Then charged particles will produce cherenkov radiation that can be detected by the LAPPD.

not customizeable.

Both of these problems are solved in the inside-configuration. All of the rapidly varying charge distributions from the electron shower produces electromagnetic fields. One can couple to these fields by placing a conductor nearby. This is the operating principle of the inside-out configuration. By placing a conductor on the outside of the detector vacuum, all of the readout can be customized external to the vacuum, in air. This configuration is shown schematically in Figure 1.2.

Such easily customizeable readouts allows for granularity, for example, by placing copper pads against the bottom of the LAPPD base. If the inner layer is a sufficiently resistive conductor, the current will die out quickly and the signal will be centered in one pad. Note the anode must still be conductive so that the excess charge can be drained to ground.

2 Occupancy Calculations in ATLAS

2.1 Rough Estimate of Necessary Pad Size

We can make a quick, rough estimate of the necessary pixel size using the empircal fact that the number of particles per collision per unit pseudorapidity [App. A] is roughly constant. CMS measured the particle flux at 13 TeV and found that there are approximately 6.2 charged particles per eta [5].

A large fraction of these particles are pions, $\pi^{\pm}$ and π^0. The $\pi^{\pm}$ will not decay and will general hit only one pixel. Thus I estimate that there are 6.2 charged pions per eta, evenly and randomly distributed in ϕ (the azimuthal angle around the beam axis). I ignore for now any correlations between particles, which will be a significant effect.

The π^0's are somewhat harder to estimate. They decay immediately into two photons, which will not directly produce a signal, unless they begin to shower in the material before the detector. In addition to the π^0's, there are other particles produced that I am ignoring. I say that all these unknowns collectively contribute a factor of 2, so that there are 21.4 charged particles per eta, randomly distributed in ϕ.

Using this information, combined with the fact that there are roughly 200 vertices per bunch crossing, it is easy to calculate the estimated number of hits in a given size pixel. I wrote a Python script to compute how many events give hits in a square pixel centered at various pseudorapidities. The results are shown in Figure 3.

This calculation was useful to determine an initial estimate for the pad size that I should use my experimental setup. It shows that to have only a fraction of events give hits in a given pixel, we need to look at pixel sizes roughly on the order of centimeters, as we can see by the length scales in Figure 3.

2.2 Simulation Method

To simulate events in ATLAS, I use Pythia [1]. Pythia is software developed in C++ to simulate Monte Carlo events at colliders. As input, it takes the center of mass energy (13

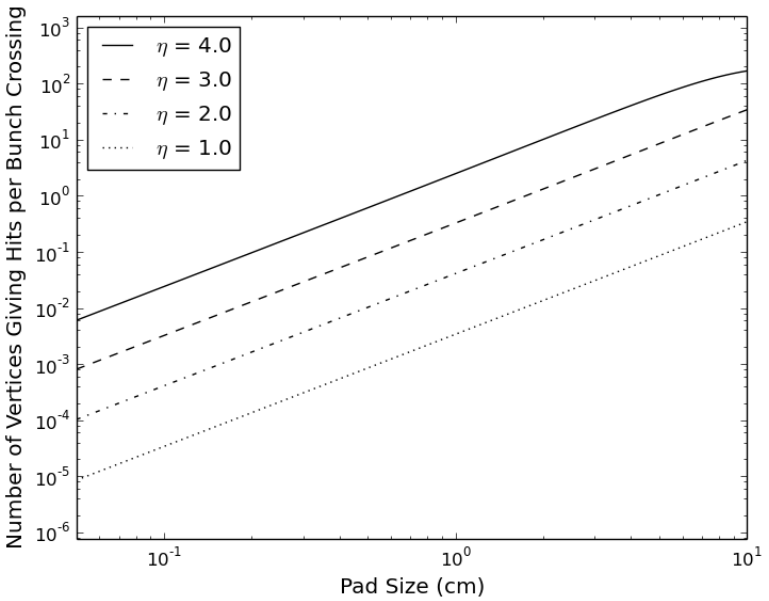

Figure 3: A crude estimate of the event occupancy as a function of square pad (pixel) size.

TeV), the composition of the beam (protons), and a set of particles sought in the final state. Then it computes the four-momenta of the final particles for a given number of events. Pythia does not account for detector effects, such as showering, but since the HGTD is to be placed before the calorimeters, there will not be much shower development when the particles reach it.

In Pythia, I generate "minimum bias" events. Minimum bias events are proton-proton collisions with no filters, i.e., not selecting for any particular final state. These are the vast majority of events at the LHC, and are not likely to contain rare "interesting" processes. Since minimum bias events are due to a variety of QCD processes, calculating them can be difficult, but Pythia is tuned to data.

Once I run Pythia, for each particle in the final state, I output to a file the four-momentum, the vertex of origin of the particle, and whether it is charged. Pythia assumes the initial interaction occurs at the origin, but it allows secondary vertices to be away from the origin. I record whether the particle is charged because photons and charged particles will behave differently. Charged particles will directly produce a signal in most detectors.

Photons, however, will only produce a signal if they have begun to shower in the material of the detector. Because Pythia does not handle detector effects, I ignore photons for the rest of the calculation. Because the HGTD is to be placed before the electromagnetic calorimeter, which is where the photon shower ideally begins, this effect should not be too large. Regardless, it could still contribute a factor of a few, which is significant when it comes to pad size. Thus my estimate will be a rough lower bound, which I will later improve.

Next, I read in the Pythia output file with Python. Since the interaction region is roughly

20 cm long, I shift the origin of each event by picking a distance from a Gaussian distribution with width 20 cm. I ignore the transverse width of the interaction region, which is small.

I also ignore the fact that not all events occur at the same time. This is again another correction. The spread in time of the events is, at maximum, the length of the interaction region. Now, the length of the interaction region already causes a spread in arrival times of 20 cm/c $\approx$ 660 ps. Assuming both distributions are Gaussian, these distribution widths will add in quadrature, resulting in an overall arrival time spread of roughly 930 ps. I plan to account for this effect in more detailed simulations, but for now, this results in another $\approx$ 40% error, on the same order as my other errors.

Now, for each event that I generate, I compute its linear trajectory. Since the HGTD is before the toroidal magnet, the particles will travel in approximately straight lines. I then determine whether the trajectory passes through a given pixel, which for simplicity I assume to be square.

To get accurate estimations of occupancies on the order of 0.01, it is necessary to use 1000 bunch crossings. I pick the number of events per bunch crossing to be Poisson distributed around 200 events. Thus I generate 250,000 events in Pythia, resulting in a 2.2 GB ASCII file listing the particle information of each event, making the occupancy calculation computationally intensive.

2.3 Figure of Merit: Event Occupancy

Using ATLAS simulations, I would like to determine what the pixel size in the HGTD needs to be such that each pixel is not overwhelmed with hits. The most immediately useful parameter is the average number of events per bunch crossing that give hits in a given pixel. We would like to get an estimate of this parameter to see whether the LAPPD's are a plausible technology for the LHC. Note that the total number of particles hitting a pixel in each bunch crossing is not particularly interesting because many particles will tend to come from the same event, and we merely want to distinguish events.

In each bunch crossing in the high-luminosity LHC, there will be approximately 200 events. We want the chance of an individual pixel hit to be small so that one pixel is not generally hit by two events in one bunch crossing. Thus the parameter of interest is the average number of events per pixel, per bunch crossing. I will call this the event occupancy.

To have the chance of a double hit be small, we want occupancies on the order of 0.01 - 0.1. With an occupancy of 0.1, assuming a Poisson distribution of events, the probability of two or more hits in one pixel in one bunch crossing is $P(\text{number of hits} \geq 2) = 4.68 \times 10^{-3}$. Similarly, for occupancy 0.01, the probability of two or more hits is $P(\text{number of hits} \geq 2) = 4.97 \times 10^{-5}$. Thus a factor of 10 reduction in occupancy results in a factor of 100 reduction in probability of a multiple hit. Therefore it is very beneficial to go reduce occupancy as much as possible.

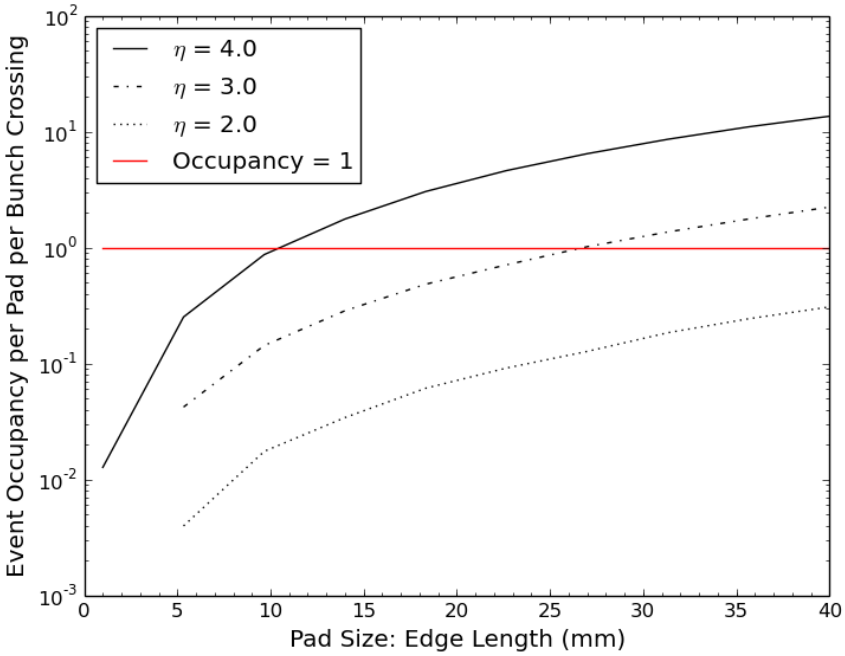

Figure 4: Occupancy as a function of pixel size for a range of η.

2.4 Simulation Results

First, I calculate the dependence of occupancy on pixel size, assuming square pixels. The results are shown in Figure 2.4. We can see that for occupancy of order 1, we need pixel size on the order of centimeters. This order of magnitude agrees with the rough estimate above, confirming that the simulation is behaving as expected.

Next, I compute the pad size necessary to achieve a given occupancy as a function of eta. I do this for occupancies of 0.1 and 0.01, since they ensure low probabilities of multiple hits per pixel. The results are shown in Figure 5.

Since the cost and complexity of the HGTD scales with the number of channels, it is economical to minimize the number of readout channels. Because the inside-out LAPPD has easily customizable pad readouts, it is easy to have pixel size depend on eta.

As an example, I arbitrarily divide the HGTD into three regions of equal width in pseudorapidity, the inner, middle, and outer regions. In practice, it may be possible to have more regions, or even to have pad size vary continuously with eta for an optimal configuration.

In each of the three regions, I compute the pixel size necessary to ensure that a specified occupancy is not exceeded. That is, I estimate the pad size as the lowest value of the curve in each of the three regions in figure 5.

Given the area of the region, this allows me to compute the number of necessary channels. Note that this calculation only considers one half of the detector. The results are shown in Table 1. As one would expect for sufficiently small pixels, a factor of 10 reduction in

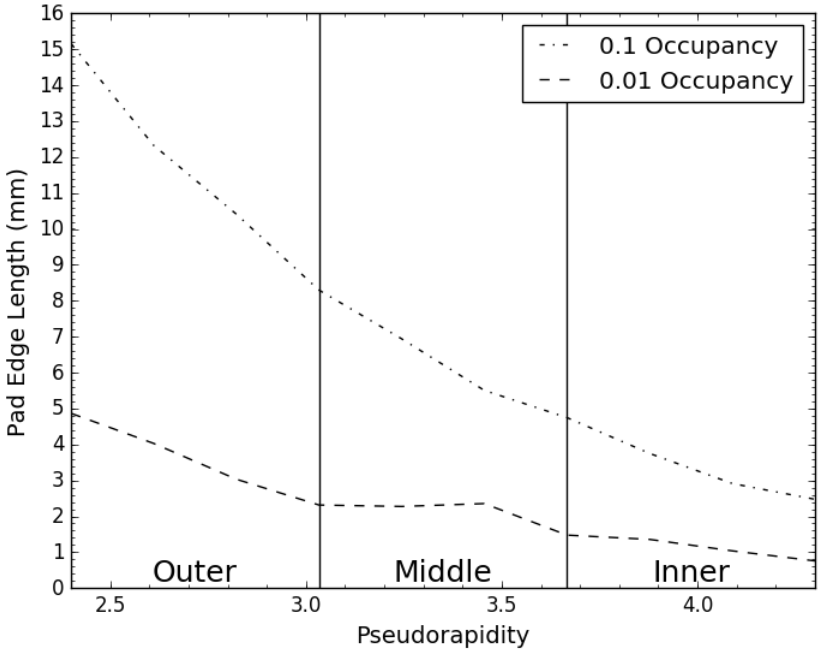

Figure 5: The necessary size of a square pixel as a function of η in order to attain a specified occupancy.

occupancy requires roughly a factor of 10 increase in the number of channels. Thus, from above, a factor of 10 increase in the number of channels results in a factor of 100 less in the probability of multiple hits in a pixel.

3 Experimental Setup

3.1 Designing and Making the Pads Printed Circuit Board with SMA Readout

Since I knew from my rough estimations that pixel size on the order of centimeters was necessary, we designed a printed circuit board where the copper pads have linear dimensions 0.5" (1.27 cm), 1.0" (2.54 cm), and 1.5" (3.81 cm). I combined these in arrays of square pads and rectangular pads, as shown in Figure 6. My simulations show that my half inch pads are plausible only for the outer region of the HGTD. Regardless, they still show the proof of principle and allow for some basic data analysis.

By having a minimum pad size of 0.5" by 0.5", I was able to solder SMA connectors directly to the bottom of the board for readout, without a more complex layered board that has readouts at the edge.

The board includes rectangular pads because it may be economical to have a different

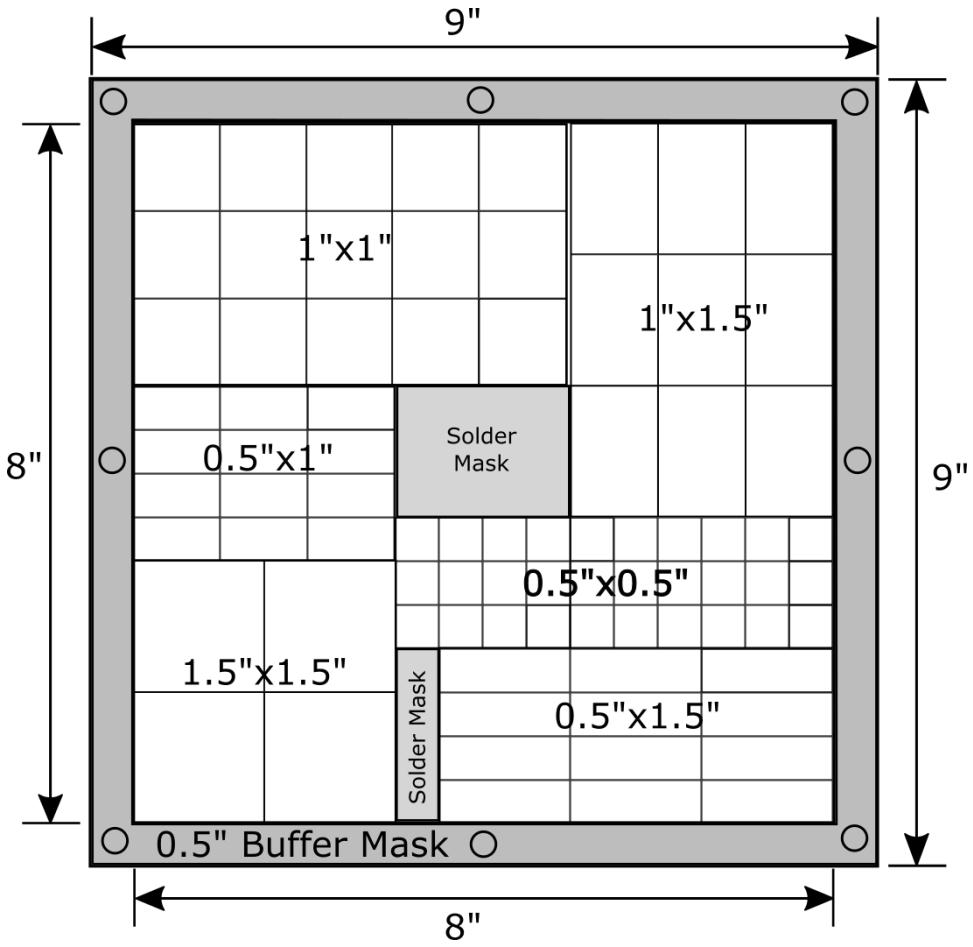

Figure 6: A sketch of the printed circuit board that I use. I left the center of the board plain solder mask so that I could press it against the ceramic if the coupling was weak and the board sagged in the middle. This was not necessary. The other narrow strip of solder mask was an artifact of fitting specific sized pads into the 8" by 8" area. On the edge of the board, I left 0.5" of solder mask so there would be room to support the board around. The circles around the edge are holes lined with copper connected to the inner ground plane for support and DC grounding with screws.

	0.1 Occupancy		0.01 Occupancy	
Rapidity Region	Pad Size (mm)	Channels	Pade Size (mm)	Channels
$2.4 < \eta < 3.0$	8.3	1.3 $\times 10^4$	2.3	1.8 $\times 10^5$
$3.0 < \eta < 3.7$	4.7	1.2 $\times 10^4$	1.5	1.7 $\times 10^5$
$3.7 < \eta < 4.3$	2.5	1.1 $\times 10^4$	0.8	1.2 $\times 10^5$

Table 1: The pad size necessary to achieve a given occupancy as a function of eta for the three pseudorapidity regions, and the approximate number of necessary channels for each region on one side of the detector. The total number of channels for the 0.1 occupancy case is 3.6 $\times 10^4$, while for the 0.01 occupancy case it is 4.6 $\times 10^5$. In comparison, an estimate in the ATLAS phase 2 scoping document [3] uses 5 mm $\times$ 5 mm pads to cover the entire region, implying a total number of channels per side of around 10^5.

pad size in eta than in phi [App. A] in the HGTD. However, the rectangular pads will not be considered in this paper, and I will focus on the 0.5" $\times$ 0.5", 1.0" $\times$ 1.0", and the 1.5" $\times$ 1.5" square pads for simplicity.

3.1.1 Readout

The experimental setup is contained in a light-tight box, a dark box, while the readout computer and electronics are external. Therefore the SMA signal cables are fed through connectors in the wall of the dark box. The signal is read with either an oscilliscope, or a PSEC board [4, 6]. PSEC is 6 channel "oscilliscope-on-a-board" that is read with a USB cable to a computer. It samples at 10 gigasamples per second and has a noise amplitude of about 0.7 mV. In our setup, it triggers on a trigger pulse from the laser, and then records data for 25 ns.

3.2 The Photodetector and Laser

In order to test the setup, we use a PLANACON^{TM} photodetector produced by Photonis [7]. The PLANACON^{TM} is an MCP-based detector with an active area of 50 mm $\times$ 50 mm. It is not as fast or as large as LAPPD's will be, but it can still be used to test the inside-out configuration.

For my setup, I power the PLANACON^{TM} at 1800 V through a voltage divider made for earlier experiments with these photodetectors.

Out light source is a picosecond diode laser produced by Advanced Laser Diode Systems [8]. It is a 405 nm pulsed laser with a repetition rate between 100 Hz and 1 MHz. The laser pulses are 500 ps in duration.

The output of the laser is a messy, large, intense beam. To fix this, we align the laser through a single mode optical fiber. The output is a small circular beam of significantly reduced intensity, so that the PLANACON^{TM} is not saturated.

The fiber optic is screwed into a holder attached to a motorized platform which can move in two dimensions. In one direction, it can only move a few centimeters, while in the other dimension it can move over 30 cm. We control the platform via an external computer so that the laser position can be moved without opening the dark box.

The entire setup is inside a dark box. The laser and its coupling to the fiber optic cable are isolated from the PLANACON^{TM} with black felt so that stray reflections do not reach it. Pictures of the setup in the dark box are shown in figure 7, without the black felt for visibility.

3.3 Inside-Out Layer: Nichrome Film

To model the inside-out layer, we use a 10 nm layer of nichrome deposited onto a ceramic. The thinness allows the electromagnetic fields to penetrate through the metal to the pads board, while simultaneously increasing the resistance so that the current pulse dies quickly and remains local.

Around the border is a 200 nm layer of nichrome for grounding. Because it is thicker, it has much less resistance. We make a DC connection to this border by clamping on a small piece of copper shim with a screw and nut. This ensures the nichrome layer is a DC ground.

The PLANACON^{TM} is coupled to the nichrome with uncured silver epoxy. We place a small, controlled dot of silver paste directly beneath the laser, grounding only this region of the PLANACON^{TM}. While this is likely results in a degredation of signal, it is the most consistent method we have found so far for ensuring the same coupling strength between different trials. Typical variations from retrying the same setup several times result in a systematic error on the pulse amplitudes of roughly 50 mV.

My final setup is shown in Figure 7.

4 Data Analysis

4.1 Pulse Shapes and Event Selection

A typical event in shown in Figure 8. The pad that the laser is centered over shows a large negative pulse, while the nearby pads show a smaller signal. Of interest is that some pads show a positive polarity, opposite the main pulse. This is evidence of the fact that directly beneath the shower there is a region of opposite charge, as explained in Section 1.3.

Unfortunately, the PSEC data is not immediately useable. The position of the pulses jitter in time over the 25 ns data collection window, so the first correction I make is to reject all events where the minimum on the largest channel does not fall within a certain window. I ensure that the pulse is not cutoff either side of the data-taking window. For example, I reject events where recording starts after the initial rise.

PSEC signals are characterized by a flat low noise period of a few nanoseconds before the pulse. The pedestal value of this noise varies between runs and to some extent between events. It is, however, the same for all channels. I created an algorithm to find this pedestal

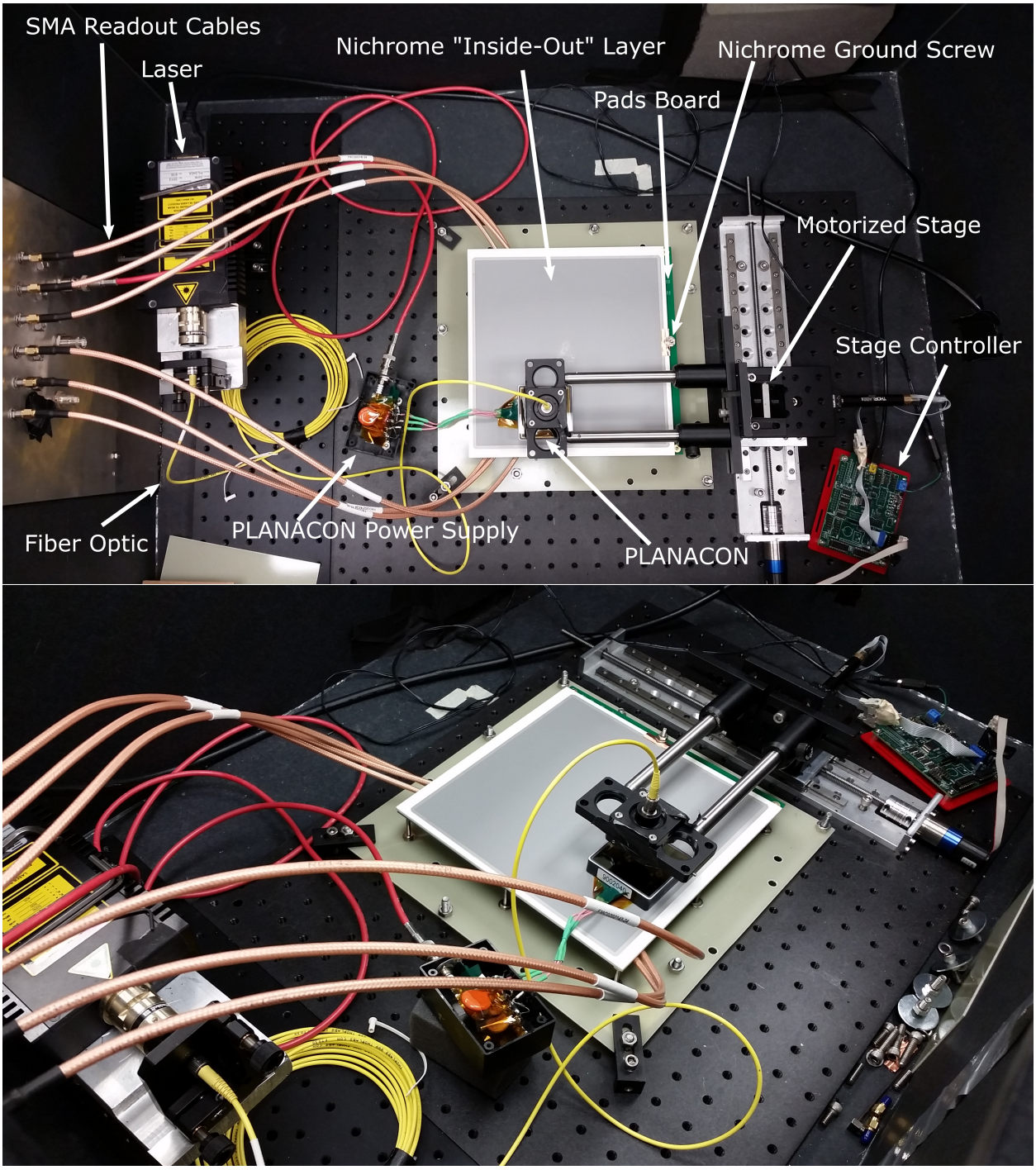

Figure 7: Pictures of my experimental setup in the dark box.

on an event-by-event basis. First I find the minimum value of the biggest peak. Then I step backwards until I reach the point of steepest slope, and construct a tangent line there. To handle the issue of noise on the rising edge, I require that the steepest point have negative slope near it since problematic noise will cause a short period of positive slope. When pulse has separated a threshold distance in x from the tangent line, I mark the point on the pulse. I call this point the "rise point" and it is the point where I say the pulse "begins." This procedure is diagrammed in red in Figure 8.

Once I have the rise point, I average the voltages of a specified number of samples before it, calling this my pedestal. Then I subtract the pedestal voltage from every sample in the pulse.

Lastly, to clean the events, I cut off data before the low-noise period before the pulse so that all pulses start at roughly the same time coordinate. Once all the pulses are aligned at roughly the same starting point, one can do a channel-by-channel average of all the pulses from a run of several thousand events. The result of this averaging is shown in Figure 9.

The average pulse is qualitatively similar to the individual pulse, though with less noise. This average pulse shows that the oscillations in the adjacent pads are not merely noise, but a ringing of the capacitances in the system that is consistent between events.

While this averaging procedure allows for estimations by eye of the average pulse amplitudes and rise times (important for time resolution), it is important that the pulses are not all exactly aligned in the average. My aligning is based on the rise point, which varies somewhat between events, introducing artificial noise. A more careful analysis below will examine these parameters in more detail.

4.2 Pulse Amplitudes

To understand how much the inside out configuration reduces the signal strength, I examine the distribution of peak amplitudes of inside-out pulses, and I compare it to data taken with the PLANACON^{TM} placed directly pads. Then, I can see how the loss from inside-out depends on pad size.

For my 1" $\times$ 1" pads, with the PLANACON^{TM} placed directly on them, I measure an average peak amplitude of 540 ± 17 mV. Testing these pads with the inside-out configuration, I find an average peak amplitude of 263 ± 7 mV. The distrubtion of pulse amplitudes for the inside-out configuration is shown in Figure 10. Thus we see that on the 1" $\times$ 1" pads, the inside-out configuration leads to a reduction in signal amplitude by a factor of 2.

4.3 Rise Times

To get a handle on the time resolution of the detector, I measure the rise times of the primary pulse. The rise time is the time it takes the pulse to go from 10% of its maximum to 90% of its maximum. Since these thresholds are usually crossed between samples, I do a linear interpolation between two samples to get exactly the crossing times. A plot of the distribution of rise times is shown in Figure 11 for the inside-out configuration on 1" $\times$ 1" pads.

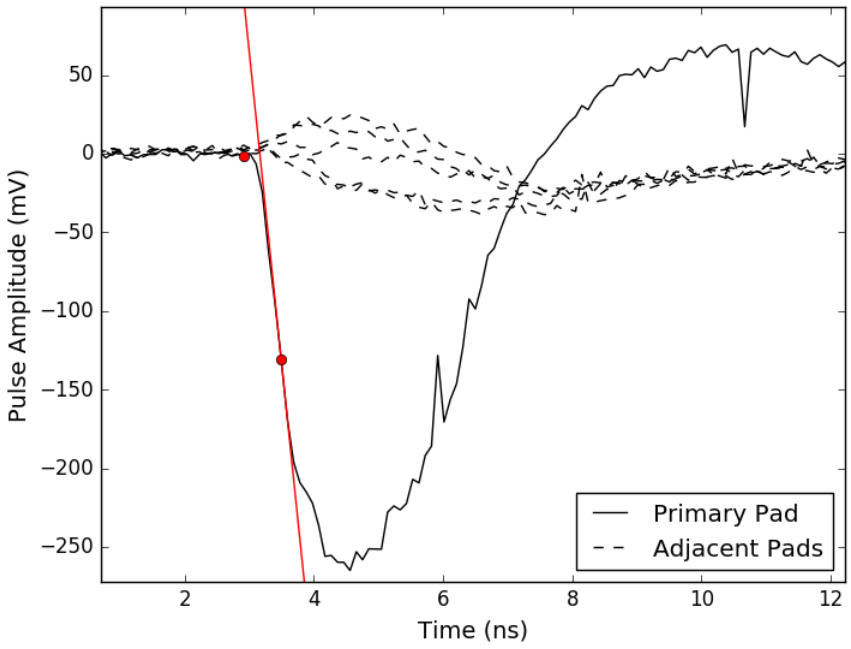

Figure 8: A typical pulse from my pads, in black. The red points and lines are used in my event selections. Data was recorded with the PSEC board. The red point along the steep rise is the steepest point. The red point at the base of the pulse is the beginning of the pulse in my algorithm. This event has been pedestal-subtracted.

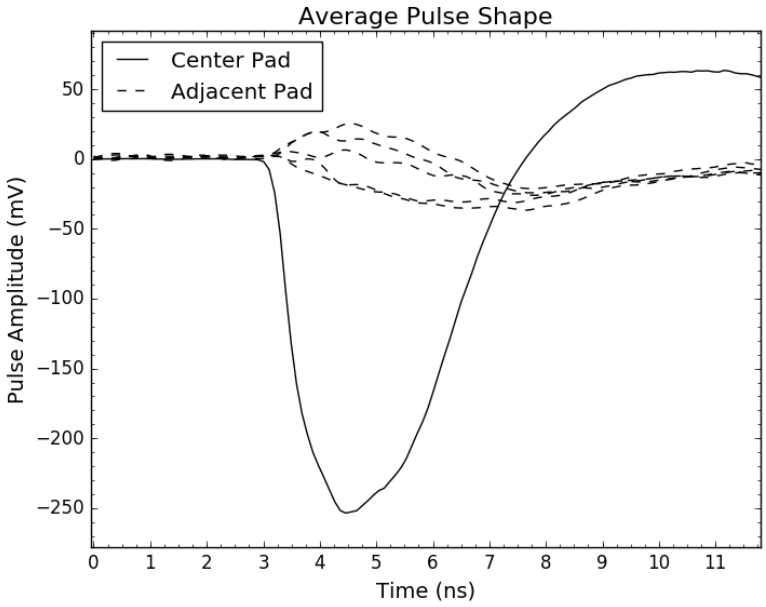

(a)

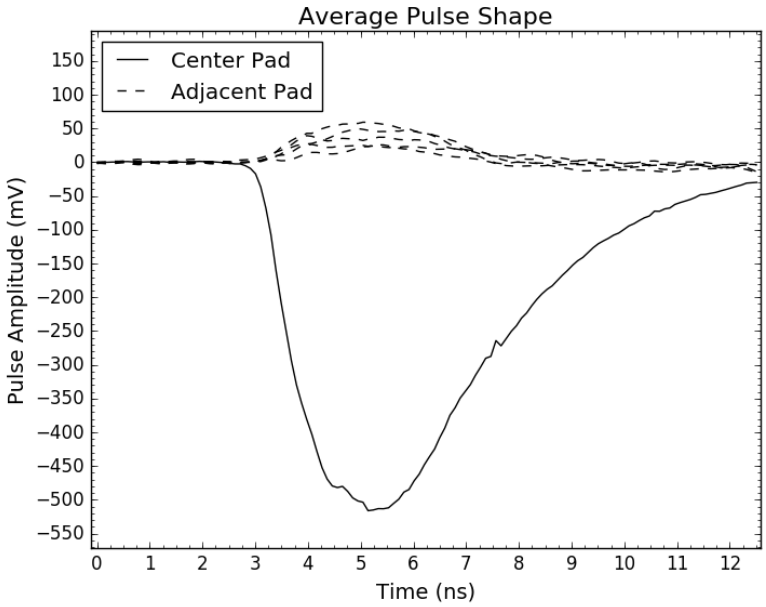

(b)

Figure 9: The average pulse shape of a dataset, where the pulses were aligned about the rise point. (a) is the inside-out configuration, while (b) is a direct signal.

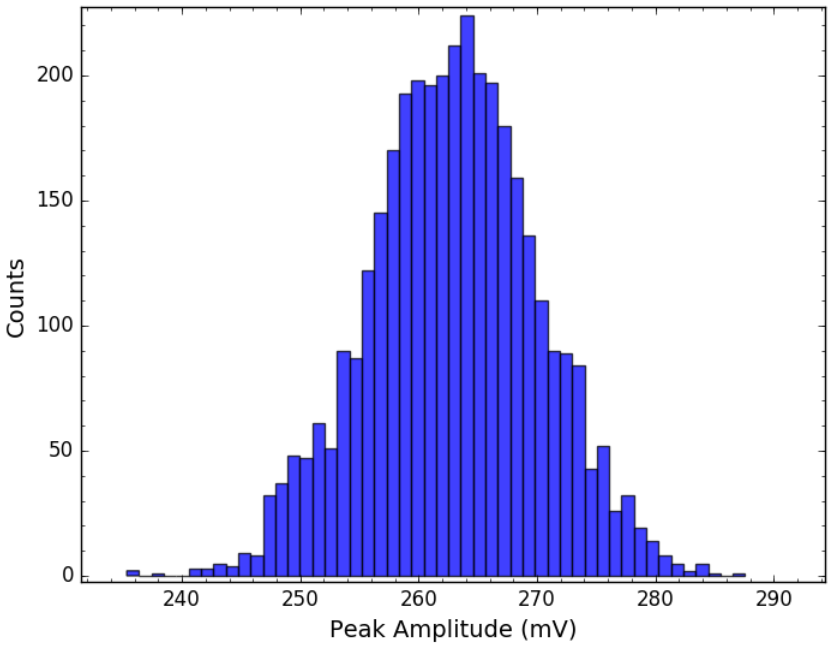

Figure 10: A histogram of the absolute value of the peak amplitudes of the primary pulses in a data set, taken in the inside-out configuration. The average is 263 mV with a standard deviation of 7 mV.

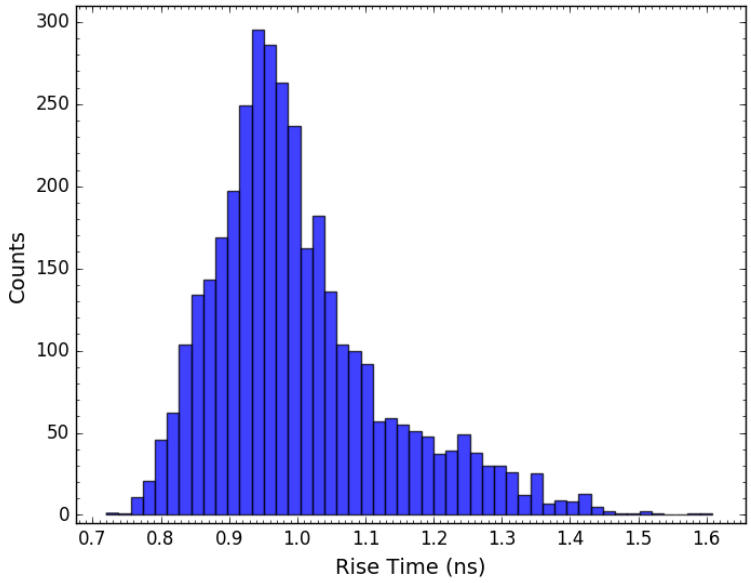

(a)

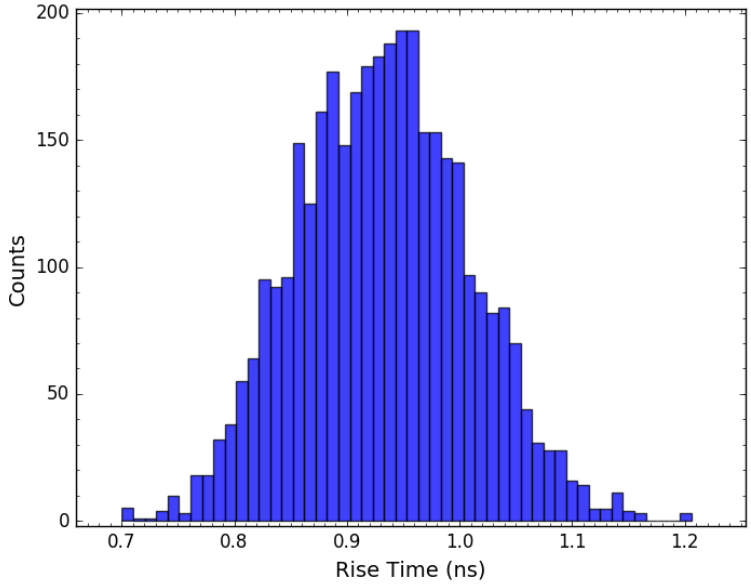

(b)

Figure 11: Histograms of the 10% to 90% rise times of the pulses in the pad directly beneath the laser, taken in the inside-out configuration with 1" × 1" pads. (a) Rise times from the first 10% crossing to the last 90% crossing. The average is 1.00 ns with a standard deviation of 0.13 ns. (b) Rise times from the first 10 % crossing to the first 90% crossing. The average is 0.93 ns with a standard deviation of 0.08 ns.

One subtlety with computation is that noise can fluctuate around the threshold. To handle this, there are two options. I can either take the first point where the pulse crosses 10% and the last point where it crosses 90%, shown in Figure 11(a); or I can take the first point where the pulse crosses 10% and the first point where it crosses 90%, shown in 11(b). In the first case, noise will bias my results toward larger rise times, which yields a more conservative rise time estimate.

When the PLANACON^{TM} is placed directly on my pads, I measure a rise time (using the symmetric calculation) of 1.23 $\pm$ 0.16 ns. The same calculation for the inside out configuration gives 0.93 $\pm$ 0.08 ns. To first order, there is not much of a difference in rise times. Importantly, the capacitance does not slow down the signal, which we would expect if the capacitance acts as a high-pass filter.

More carefully, the rise time for the inside-out configuration is actually faster than for the direct configuration. This is likely related to the fact that the amplitude is less for the inside-out configuration. A plausible explanation is that negative ringing pulls the inside-out pulse back toward zero before it has reached the same peak as the direct signal. This would reduce the amplitude, as well as cut short the rising edge. This hypothesis is supported by the fact that the inside-out configuration has a large swing-back after the pulse, a feature that is not seen in the direct configuration.

5 Conclusions

5.1 Inside-Out Photodetector Performance

In summary, we have demonstrated that the inside-out configuration is extremely feasible. Signal amplitudes are reduced by only a factor of order 2 on my 1" $\times$ 1" pads. Furthermore, the rise time, and therefore the time resolution, does not seem to be significantly affected by the new configuration. This is likely because inside-out acts as a high pass filter.

Another important feature is that signal in adjacent pads is small compared to the central pad, and in particular, they have opposite polarity. Thus two hits in adjacent pads should be distinguishable from one hit in one pad. Since a single hit does not induce signals in far-away pads, it should be possible to operate in high event rate environments. The pads indeed seem to function independently.

5.2 Feasibility for ATLAS

Thus far, there do not appear to be any major obstacles for using LAPPD's for fast timing in the forward region at ATLAS. The number of channels that I estimate to be necessary to handle the particle flux is reasonable, and the sizes of the pixels are achievable.

One possible as-of-yet untested issue is that the inside-out configuration could have a minimum possible pad size comparable to the required pixel size. That is, it is possible that pads with a certain size (5 mm $\times$ 5 mm, for example) do not have such a clean central pad signal, and adjacent pads would have similar amplitude. What pad size this happens at is

determined by the distance scales of the shower and induced charges, which has not been tested. All that is known is that it is less than an inch.

5.3 Future Tasks

Though much has been tested, much work remains to do. First, I would like to have more accurate calculations of necessary pad sizes in ATLAS. Importantly, this requires accounting for photon signals, and for the time distribution of events.

I also plan to test different pad sizes. It will be interesting to see how signal amplitude and rise time depends on pad size. I will also be able to test whether 0.5" $\times$ 0.5" pads have a strong a decoupling between pads as the 1" $\times$ 1" pads do.

To get some handle on shape and size of the inside-out electromagnetic pulse, I will perform a position scan over the 0.5" $\times$ 0.5" pads. By measuring how the signal amplitude varies as the laser is scanned across a pad, it should be possible to understand the minimum possible pad size.

Further goals include making a rough design of a possible setup for use in ATLAS, and determining whether a fast-timing forward detector would allow for measurement of the interesting physics of Higgs vector boson fusion in the forward region.

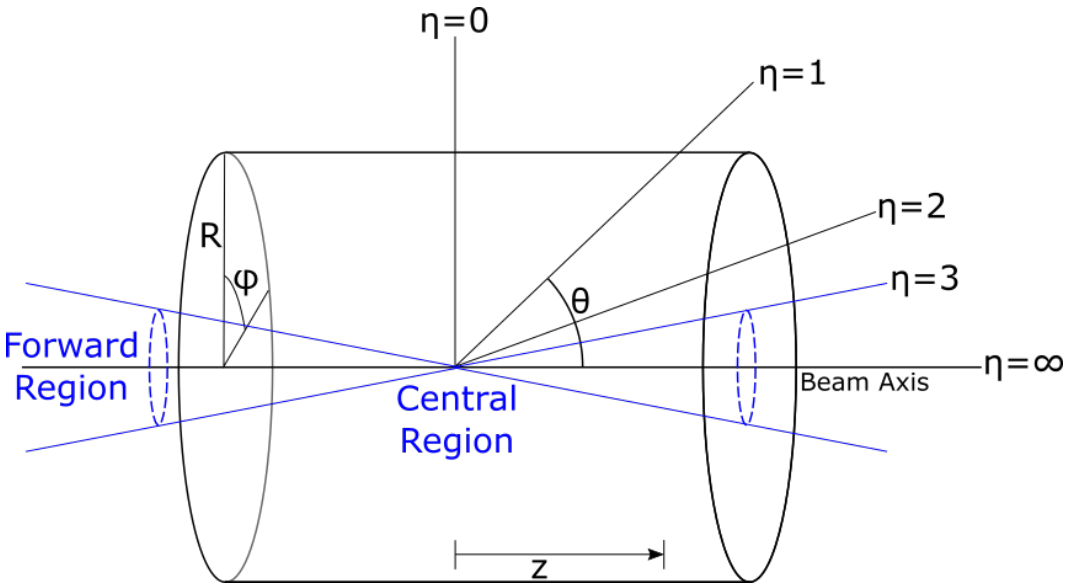

Figure 12: A sketch of the detector variables. The cylinder is the detector, and the center-point is the center of the detector, in the center of the interaction region.

Appendices

A Collider Detector Terminology

This is a short list of the important variables and terms in collider detector physics. Many of the below variables are shown in Figure 12.

- Bunch Crossing: Proton beams in the LHC circle in many (order of 1000) clumps of protons called bunches. For collisions, two oppositely-traveling bunches are brought to cross inside a detector. There are many (order of 20-200) proton-proton collisions per bunch crossing.
- Central Region: The region of the detector perpendicular to the beam. It has small pseudorapidity, rough $|\eta| < 3$.
- Event: An event is a single proton-proton collision and all the particle tracks coming from it.
- Forward Region: The region near the beam axis. It has large pseudorapidity, roughly $|\eta| > 3$.
- Longitudinal Direction: The direction along the beam.
- Phi (ϕ): The angle around the beam axis, the usual cylindrical angular coordinate.

- Pseudorapidity (η): Pseudorapidity is defined as $\eta = -\ln[\tan(\frac{\theta}{2})]$. $\eta = 0$ directly transverse to the beam, and $\eta \to \infty$ along the beam axis.
- R: The radial distance from the beam axis.
- Theta (θ): The angle up from the beam axis. The spherical polar anglular coordinate.
- Track: The reconstructed trajectory of a particle.
- Transverse Direction: The direction perpendicular to the beam.
- Vertex: Generally, a vertex is the point that particle tracks trace back to. The primary vertex is the collision point of two protons. Secondary vertices are points where semistable particles decay inside the detector near the interaction region.
- Vertexing: Accurately identifying which vertex corresponds to which particle tracks. This involves discriminating different vertices with either a high position or time resolution.
- z: The distance along the beam axis from the center point.

References

[1] T. Sjstrand, S. Mrenna and P. Skands, JHEP05 (2006) 026, Comput. Phys. Comm. 178 (2008) 852.

[2] The ATLAS Experiment at the CERN Large Hadron Collider. *J. Instrum.*, 3:S08003. 437 p, 2008. Also published by CERN Geneva in 2010.

[3] ATLAS Phase-II Upgrade Scoping Document. Technical Report CERN-LHCC-2015-020. LHCC-G-166, CERN, Geneva, Sep 2015.

[4] B. W. Adams et al. A Brief Technical History of the Large-Area Picosecond Photodetector (LAPPD) Collaboration. 2016.

[5] Vardan Khachatryan et al. Pseudorapidity distribution of charged hadrons in proton-proton collisions at $\sqrt{s} = 13$ TeV. *Phys. Lett.*, B751:143–163, 2015.

[6] Eric Oberla, Jean-Francois Genat, Herve Grabas, Henry Frisch, Kurtis Nishimura, and Gary Varner. A 15 GSa/s, 1.5 GHz bandwidth waveform digitizing ASIC. *Nucl. Instrum. Meth.*, A735:452–461, 2014.

[7] Photonis. Planacon^{TM}. See the Photonis website http://www.photonis.com/en/product/ for more information.

[8] Advanced Laser Diode Systems. Picosecond diode laser = pilas. See the website for more information, http://www.alsgmbh.de.

Acknowledgements

There are many people who helped me immensely throughout this work. First, I would like to thank Evan Angelico. Our projects closely paralleled each other, and it was thanks to his experimental knack that the setup was able to move as quickly as it did.

I'd like to thank Bernhard Adams, who was immensely helpful in setting up the laser, for providing the motorized stage, and for other general assistance. Also, I'd like to thank Tang for assisting with the design and fabrication of the pads board, Eric Oberla for helping us operate and debug the PSEC board, and Mark Zaskowski for helping with various mechanical tasks.

Additionally, thanks to Jim Pilcher, Mel Shochett, and Mark Oreglia for being excellent resources in learning about ATLAS.

Lastly and most importantly, I'd like to thank my adviser Henry Frisch for providing an interesting project, being an excellent guiding hand, and a knowledgeable resource.